The anaerobic corrosion of candidate disposal canister materials in compacted bentonite exposed to natural granitic porewater containing native microbial populations

B. Reddy[1], C. Padovani[1], A.P. Rance[1], N.R. Smart[1], A. Cook[1], A.E. Milodowski[2], L.P Field[2], S.J. Kemp[2], A. Martin[3], N. Diomidis[3]

[1] Wood, HQ Building, Thomson Avenue, Harwell Campus OX11 0GD, United Kingdom.

[2] British Geological Survey, Keyworth, Nottingham, NG12 5GG, United Kingdom

[3] Nagra, Hardstrasse 73, Postfach 280, 5430 Wettingen, Switzerland

Corresponding author: nikitas.diomidis@nagra.ch

The Materials Corrosion Test (MaCoTe) is a long-term, multi-national *in situ* corrosion experiment set up at the Grimsel Test Site, Switzerland. The experiment has been operating since 2014 with a focus on the corrosion behaviour of container materials for the disposal of high-level waste and spent nuclear fuel under conditions representing a granitic deep geological repository. The experiment consists of eight modules containing metal coupons and bentonite. Two of the modules, each with a different bentonite density, have been retrieved after 394 days of exposure and have been analysed using a range of techniques aimed at studying the corrosion behaviour of the metals and the mineralogical evolution of the bentonite. Weight loss measurements show that carbon steel had a relatively low average corrosion rate ($\sim 2 \, \mu m \, yr^{-1}$). Much lower average corrosion rates were measured for the various types of copper (0.13 to 0.32 $\mu m \, yr^{-1}$). No detectable corrosion was measured on stainless steel coupons. To date, no significant differences were observed in the corrosion behaviour and rate of the test metals in bentonite with different dry densities.

Keywords: Copper, carbon steel, stainless steel, anaerobic, corrosion, microbial, bentonite, waste

1 Introduction

Deep geological repositories are the internationally accepted solution to the disposal of radioactive waste since they isolate the waste from the biosphere for very long timeframes [1]. A geological repository is a multi-barrier concept consisting of a host rock, a buffer, a disposal canister, and the waste form [2, 3]. Bentonite is often selected as a buffer material because, among other desirable properties, it has a low permeability thus reducing the flow of groundwater and corroding agents reaching the waste containers, and that of radionuclides released from the waste into the environment after perforation of the waste containers [4]. Several metals including carbon steel, copper, and stainless steel are being considered for use as container materials for the disposal of spent fuel (SF) and high-level waste (HLW). In the anoxic conditions expected in the repository, and with suitable engineering measures (i.e. choice of container and buffer materials and suitable dimensioning), engineered barrier systems making use of such materials are expected to provide in situ containment of the radionuclides and harmful species present in the waste for very long periods of time [5, 6]. Several factors may influence the extent to which the containers will corrode, including: (i) a failure to emplace the bentonite at a suitable (target) density [7], (ii) the bentonite density decreasing over the duration of the repository lifetime due to erosion processes [8], and (iii) microbial cells in the groundwater and bentonite becoming or remaining active during prolonged periods after disposal and producing corroding agents such as sulphide ions [9]. Microbial activity is also inherently linked to bentonite density, with a sufficient bentonite density inhibiting the growth, and activity of microbial cells [10].

The Materials Corrosion Test (MaCoTe) is a multi-national experiment conducted as collaboration between several radioactive waste management organizations and research entities across the world, namely Nagra (Switzerland), NWMO (Canada), RWM (UK), SURAO (Czech Republic), NUMO (Japan), KIT (Germany) and KIGAM (South Korea). It aims to investigate the corrosion behaviour of candidate canister materials under conditions relevant to the disposal of radioactive waste in a repository constructed in a granitic host rock with bentonite as buffer. The experiment consists of eight stainless steel modules, each containing bentonite and several metal coupons made of a range of materials. All modules are emplaced in a single anoxic borehole at the Grimsel Test Site (GTS), Switzerland. The experiment was initially set up in 2014, with modules being retrieved and replaced on a periodic basis. The overall objective of the experiment is to provide measurements of the in situ corrosion rate of stainless steel, carbon steel and different forms of copper and copper coatings, while studying the effect of the bentonite buffer density on microbial activity and microbiologically influenced corrosion (MIC). Two different densities of bentonite are employed, one representing well emplaced bentonite, and one simulating altered bentonite (for example due to thermal or chemical alterations) or bentonite that was not emplaced at the target density. The evolution of microbial activity in the bentonite and the surrounding groundwater within the same experiment discussed in this paper is presented in Engel et.al. [11]. This paper focuses on corrosion of the container materials, the corrosion products produced, and any resulting alteration of the bentonite. A similar experiment is being conducted in Opalinus Clay host rock at the Mont Terri underground laboratory, Switzerland [12, 13, 14, 15, 16], and the results between the two tests are compared. Other in situ corrosion tests in a granitic environment, but with different type of test modules, have been carried out in Äspö Hard Rock Laboratory (HRL) in Sweden [17, 18, 19, 20].

2 Experimental Details

2.1 Experimental set-up

The experimental set-up consists of a single, vertical-descending borehole which is sealed from the environment with a double packer system. In the borehole, several modules containing metal coupons and bentonite are exposed to natural granitic porewater under anoxic conditions, as shown in Figure 1. The external dimensions of the modules are 250 mm length with a diameter of 126 mm. The walls of the module contain holes allowing the ingress of groundwater. A liner is used inside the module to control the initial volume and resulting swelling of the bentonite (3 mm thick cylindrical sintered stainless steel filter with an average pore size of 18 µm and a porosity of 30%). The experimental set-up and module design is practically identical to the one used in the IC-A experiment at Mont Terri [13], allowing for comparisons between clay and granitic host rocks and associated groundwaters.
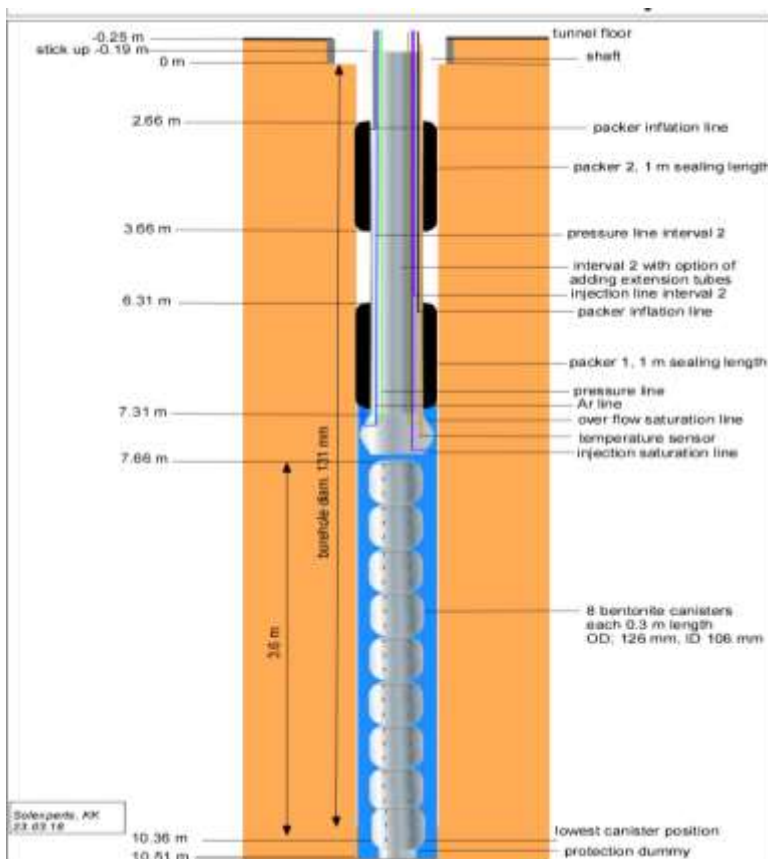
Figure 1. MaCoTe experimental layout at the Grimsel Test Site (GTS).

2.2 Preparation of bentonite

Volclay MX-80 bentonite was used in this experiment. Mixtures of different dry densities were prepared by mixing bentonite pellets and powder. A 1250 kg m^{-3} bentonite dry density was used to represent an improperly emplaced, or degraded bentonite barrier, and a 1500 kgm^{-3} bentonite dry density was used to represent the target density for a well-functioning bentonite buffer. Each module contained 12 coupons separated in 4 layers of 3 coupons each. The weight of bentonite was calculated based on a water content of 6.4%. The volume of each bentonite layer was measured in a 1 litre measuring cylinder, and weight discrepancies between the cylinder weight and the target weight were corrected using powdered bentonite emplaced between the pellets.

2.3 Preparation of coupons

Three types of test metals were used in the experiment: carbon steel, copper and stainless steel. The carbon steel was part of a partial canister prototype with an electron beam welded lid fabricated by The Welding Institute, UK (TWI), who heat-treated and cut the carbon steel cylinder into sections. The carbon steel grade was ASTM A694-08 F65 (composition, wt-%: C 0.11; Mn 1.3; Si: 0.20; P 0.010; Si 0.002; Cr: 0.10; Ni 0.07; Mo 0.17; V 0.053; Nb 0.037; Fe bal.). Electrodeposited copper (Nanovate TM C4010 [21]), and cold-sprayed copper [22] were provided by Nuclear Waste Management Organisation, Canada (NWMO). Oxygen-free phosphorus-doped wrought copper (SKB, Sweden [23]) was used as reference. Stainless steel (Duplex 2205, hot rolled, coil-plate finish) was provided by the Czech Radioactive Waste Repository Authority (SURAO) in the form of 20 mm diameter coupons with a 3 mm thickness. All coupons were ultrasonically cleaned in acetone, and grit-blasted with 120/220 grade aluminum oxide powder. The grit-blasting of the coupons provided a consistent surface roughness (R_a) of ~0.5 µm, measured using a Talysurf instrument on a representative 10% sample. Further ultrasonic cleaning was carried out after the grit-blasting and the coupons were weighed twice to a precision of 0.00001g. Coupons were photographed for additional traceability.

2.4 Assembly and emplacement of corrosion test modules

The module housing and associated sintered filters were cleaned with acetone and deionized water. The layout of the coupons in the module are shown in Figure 2.

Figure 2. Illustration of stainless steel module and its contents, including layout of coupons. The thickness of the cylindrical coupons is given in parentheses.

The modules were assembled in air, with the contents of the modules being secured with a lid after emplacement. The modules were then placed in an anaerobic glovebox, where they were pre-saturated with natural, anoxic, Grimsel groundwater by placing them in water-filled plastic containers for 10 days.

The modules were then sealed in three layers of Mylar™ bags to maintain an anoxic (argon) atmosphere during transport. They were emplaced in the borehole at the GTS, Switzerland while continuously flushing with argon gas to maintain anoxic conditions. During transport, some of the bags were damaged and, as a result, these modules may have been exposed to aerobic conditions for a maximum period of 20 days before emplacement in the borehole. The modules described in this paper were emplaced at the GTS on 22 September 2014. The chemical composition of the borehole groundwater was measured prior to the emplacement of the modules and is given in reference [24]. The temperature of the groundwater at the time of the module emplacement in the borehole was 13 ℃ and a pH of 8.4.

2.5 Module retrieval and analysis

The modules were removed from the borehole at the GTS, Switzerland on the 21 October 2015 after a total exposure duration of 394 days. The borehole was purged with argon gas during module removal to ensure an anoxic environment was maintained. Once extracted from the borehole, the modules were placed in bespoke leak-tested transfer flasks along with a small volume of borehole groundwater. The transfer flask lids were sealed, and argon gas was bubbled through an integral dip tube for 30 mins to ensure anoxic conditions were maintained during transport. A bubbler containing porewater was also connected to the outlet of the transfer flasks to prevent air ingress. Dismantling of the modules and extraction of coupons and bentonite samples for analysis was done in a pre-cleaned and sterilized argon-purged glovebox. The extraction of the coupons from the bentonite was done by fracturing, at the metal-bentonite interface. This led to some of the corrosion or alteration products remaining attached to the coupon and some on the bentonite. Both sides of the fractured interface were analysed.

2.6 Characterization of metal coupons

Post-mortem characterisation of the corrosion coupons (Raman spectroscopy, XPS and SEM analysis) was carried out at the Oxford University Materials Service. Weight loss measurements were carried out at Jacobs Harwell laboratories. Profilometry was carried out at the University of Manchester. When transported, samples were shipped inside airtight containers sealed under argon. The materials were stored inside such containers up to just before the analysis, thus minimising exposure to air.

2.6.1 Surface characterisation

A JEOL 6480 LV SEM equipped with an Oxford Instruments X-MAX80 SD X-ray detector and INCA X ray analysis system was used to image the samples and perform EDX analysis. The settings used were 15 kV under high vacuum conditions. Images, elemental maps and line-scans were acquired.

A Horiba JY LabRam Aramis confocal Raman microscope, with an exciting laser wavelength of 532 nm, was used to carry out Raman analysis. Tests were carried out on fully-sealed samples through the use of a laser-transparent glass window without exposure to air.

XPS analysis was carried out to determine the surface composition and the oxidation state of the predominant species. Samples were analysed using a Thermo Scientific K-Alpha XPS instrument equipped with a micro focused monochromated Al X-ray source. The source was operated at 12 keV and a 400 µm spot size was used. The analyser operates at a constant energy (CE) of 200 eV for survey scans and of 50 eV for detailed scans. Charge neutralization was applied using a combined low energy / ion flood source.

Data acquisition and analysis are performed using Thermo Scientific Avantage software. Peak fitting (Lorentzian / Gaussian, L/G 30%) was applied following removal of a Smart background. Normalised atomic percentages are determined from peak areas of the elemental main peaks detected on the survey scan following background subtraction and application of sensitivity factors.

Depth profiling is achieved using 2 kV Ar^+ ions at the medium current setting, which is equivalent to an erosion rate of ca. 1 nm min^{-1}. Profiles are obtained in 10 steps with 20s ion bombardment per step, for a total depth of 3.3 nm.

2.6.2 Cross-section characterization

For SEM/EDX cross sections, the coupons were mounted using an epoxy-based resin and then cross-sectioned manually with a hack saw. Half of each sectioned coupon was mounted in epoxy-based resin and ground and polished flat. Where possible, the samples were kept under vacuum in between preparation steps. Prior to SEM/EDX analysis the samples were carbon-coated to reduce charging and image distortion during analysis.

A JEOL 6480 LV SEM equipped with an Oxford Instruments X-MAX80 SD X-ray detector and INCA X ray analysis system was used to image the samples and perform EDX analysis. The settings used were 15 kV under high vacuum conditions. Images, elemental maps and line-scans were acquired at the interfaces between the metal and the surrounding bentonite.

2.6.3 Weight loss and profilometry

The corrosion rate of coupons was determined using weight loss measurements according to standard practice ASTM G1-03 [14]. Clarke's solution (inhibited hydrochloric acid) and hydrochloric acid (50 vol%) were used as descaling agents on the carbon steel coupons and the copper coupons respectively [25]. For stainless steel samples, Clarke's solution was used initially and resulted in no apparent loss of weight; subsequently a 20% HNO_3 solution (as suggested in ASTM G1-03 [25] was used to carry out some additional measurements with no loss of weight either.

For carbon steel and stainless steel only two exposures were carried out (i.e. the first exposure was sufficient to remove all the corrosion product, the second was used to correct the first to take into account the corrosion rate of the bare metal in the descaling agent). For copper coupons the process was repeated until a clear change in slope of the weight loss graph (i.e. weight loss vs. number of descaling steps) could be determined, indicating that all the corrosion product had been removed. Additional details about the procedure used for copper are available in [13]. Corrosion rates were determined from weight loss measurements on these coupons in accordance with procedure ASTM G1-03 [25]. The weight loss was converted into an 'average' corrosion rate given in units of $\mu m \ yr^{-1}$. This average reflects both a geometric average (the value obtained if all the surface corroded uniformly) and a time average (the value obtained if the surface corroded at the same rate throughout the experimental duration).

Profilometry of the coupons was carried out after the weight loss measurements to evaluate the surface topography of the metal. These tests were carried out using a confocal laser scanning microscope (Keyence VK-X200). An area (~3.3×4.5 mm) on one flat side of the coupons was mapped through the acquisition and stitching of 49 separate maps, with a vertical resolution of 0.5 µm. Roughness parameters were calculated for ten individual line profiles across these maps in both the horizontal and vertical directions. For comparison, measurements on pristine samples (i.e. coupons which had not been exposed) were also taken.

2.7 Analysis of bentonite

Mineralogical and microchemical investigations were carried out at the British Geological Survey (BGS). Two samples of bentonite (density 1500 kg m^{-3}) in contact with either carbon steel or wrought copper were analysed using XRD and petrographical analysis. The bentonite blocks within the module were subsampled in an argon-purged glovebox. The -samples were sealed in heat-welded plastic bags (triple-bagged), which were filled with oxygen free argon inside the glovebox. Bentonite samples taken next to the coupons were compared to a reference sample taken from the same module but away from any metal and subjected to the same sampling regime.

XRD analysis of bentonite was achieved by collecting bentonite chips with a scalpel and disaggregating them with a clean agate pestle and mortar. A fine bentonite powder was immediately loaded into a front-loaded cavity mount for random-oriented powder XRD analysis. Material for oriented XRD mounts was prepared by dispersing ~15 mg portions of bentonite in deionised water using an ultrasound treatment and no dispersant. The dispersions were pipetted onto glass slip substrates and allowed to dry at room temperature overnight.

3 Results

3.1 Corrosion rate

The average corrosion rates for the exposure period of 394 days are shown in Figure 3. The corrosion rate of carbon steel ranged from 1.87 µm yr^{-1} to 2.05 µm yr^{-1}, while the corrosion rates for the various copper coupons were much lower and the corrosion rate of stainless steel was negligible. At a bentonite density of 1250 kg m^{-3} the cold-sprayed copper had an average corrosion rate of 0.17 µm yr^{-1} whilst the electrodeposited and wrought copper had an average corrosion rate of 0.24 µm yr^{-1}. At a bentonite density of 1500 kg m^{-3}, copper average corrosion rates were between 0.09 and 0.21 µm yr^{-1}, with upper uncertainty levels of approximately ±0.5 µm yr^{-1}. Note that, as a result of successful developments in the weight loss methodology, uncertainties calculated for copper samples extracted from the module with a bentonite density of 1250 kg m^{-3} were lower than those calculated for copper samples extracted from the bentonite with a density of 1500 kg m^{-3}, which were used in initial trails. This is not expected to reflect differences in corrosion behaviour between the two bentonite densities, only differences in methodology used to evaluate uncertainty.
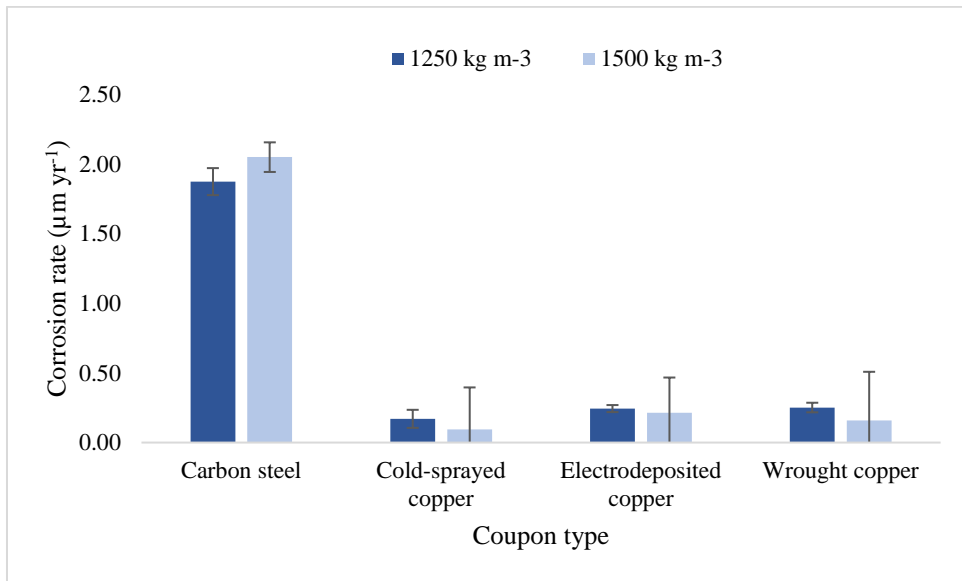
Figure 3. Average corrosion rates for carbon steel, and cold sprayed, electrodeposited and wrought copper in bentonite with densities of 1250 kg m^{-3} and 1500 kg m^{-3} after a nominal exposure period of 394 days.

3.2 Profilometry measurements

The profilometry measurements for pristine coupons and coupons after exposure are shown in Figure 4. For all materials, the roughness after exposure were similar to those of pristine samples, indicating pitting or surface roughening did not occur or was minimal.
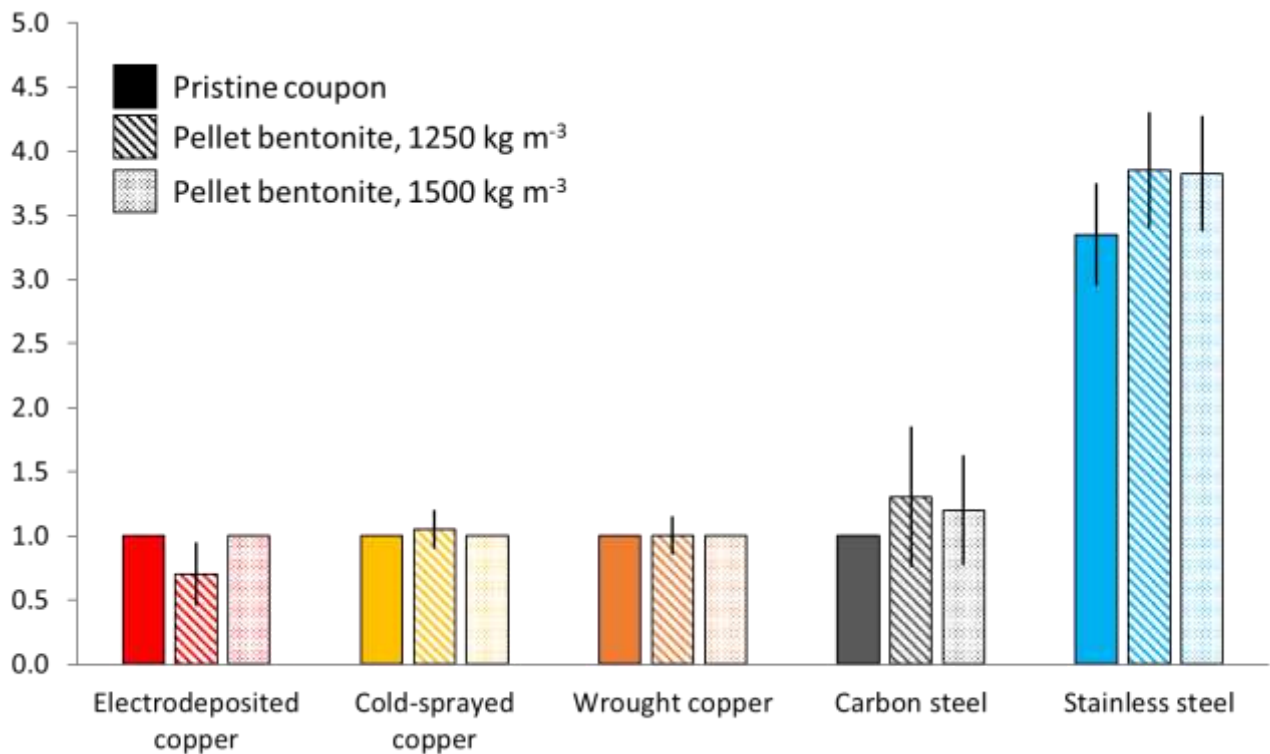
Figure 4. Average roughness (Ra) values for pristine coupons and coupons exposed in situ for a nominal duration of 394 days within bentonite with a dry density of 1250 and 1500 kg m^{-3}.

3.3 Surface characterization

Optical images of carbon steel, copper and stainless steel coupons before and after exposure are shown in Figure 5. The carbon steel coupons showed a widespread greyish/black colour and, in some areas, brownish colouration. Copper samples showed reddish colouration on top of an otherwise metallic-copper surface. Stainless steel samples looked darker but closer inspection suggested that such darkening was associated with adhering bentonite.
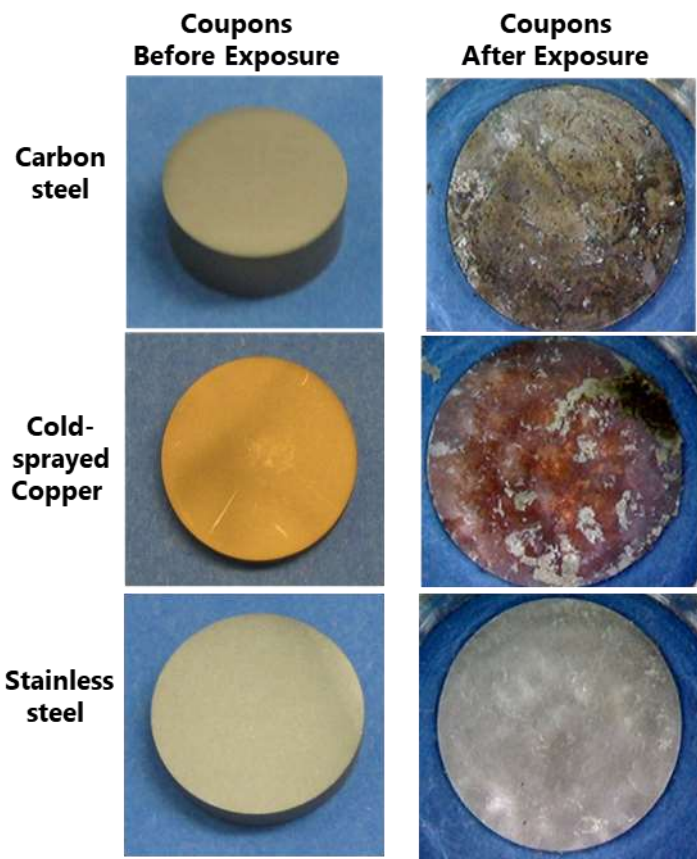
Figure 5. Optical images of carbon steel, stainless steel and copper coupons before and after in situ exposure for 394 days to bentonite with a density of 1250 kg m^{-3}.

SEM and EDX analyses were carried out on a selection of copper, stainless steel and carbon steel coupons removed from the modules. Data collected on carbon steel and copper are shown in Figure 6 and Figure 7 respectively. As expected from the optical images, the surface of all materials was inhomogeneous with some areas appearing darker under the SEM which consisted of adhering bentonite (Si, Al, O).

In the case of carbon steel, the areas not covered with bentonite (brighter under the SEM) showed greater amounts of iron and oxygen, suggesting the presence of iron corrosion products or bentonite alteration phases containing iron. In the case of copper, in some spots Al and O are present in the absence of Si which seems to be correlated to surface preparation with grit blasting with alumina particles. Other areas (brighter under the SEM) were characterised by a strong copper signal. In the case of stainless steel (not shown), apart from areas containing elements typically associated with bentonite, no others sign of surface alteration where found. For all metals, there were no significant differences between coupons exposed in bentonite with different densities.
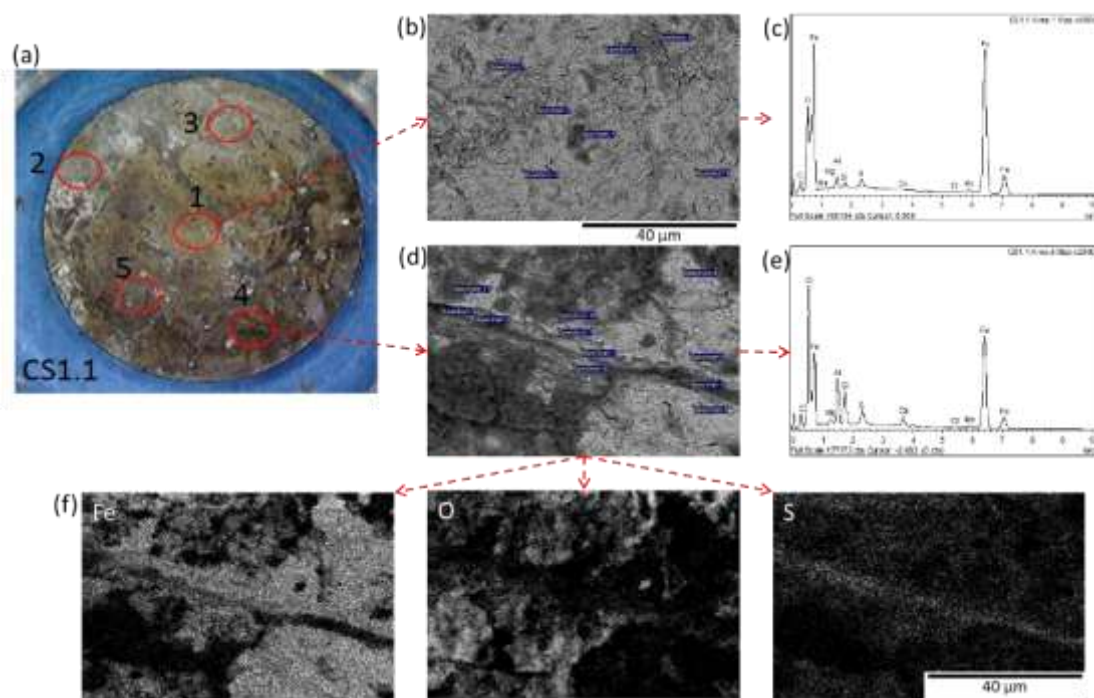
Figure 6. SEM-EDX analysis of carbon steel after in situ exposure for 394 days to bentonite with a density of 1250 kg m^{-3}; (a) optical image of coupon, with analysis areas marked; (b, d) backscattered electron image of areas 1 and 4; (c, e) overall EDX spectrum of areas 1 and 4; (f) elemental maps acquired from area 4.
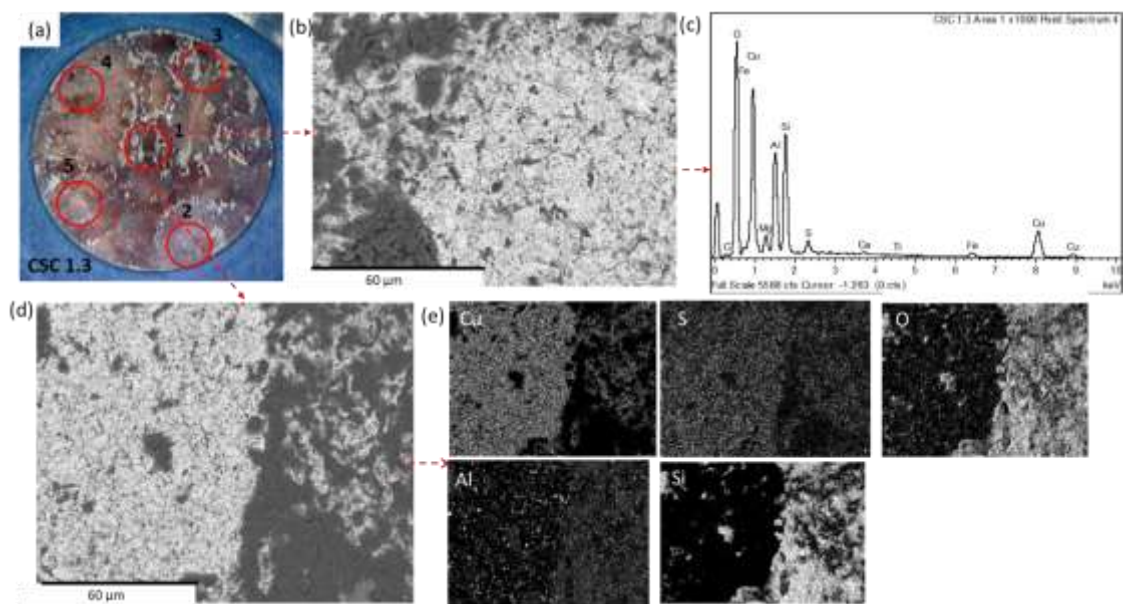
Figure 7. SEM-EDX analysis of cold sprayed copper after in situ exposure for 394 days in bentonite with a density of 1250 kg m^{-3}. (a) optical image of coupon, with analysis areas marked. (b, d) backscattered electron image of areas 1 and 4; (c) overall EDX spectrum of area 1, (e) elemental maps acquired from area 4.

Raman spectra obtained from several areas on a carbon steel and on a wrought copper coupon are shown in Figure 8. For carbon steel, the main peaks observed were centred at 300 cm^{-1} (attributed to haematite, and/or possibly FeOOH), 700 cm^{-1} (attributed to magnetite) and a doublet peak in the 1200-1600 cm^{-1} region, which could potentially be attributed to the presence of graphite or iron-carbide [26]. The spectra for different areas of the wrought copper coupon were very similar, with a number of peaks in the 100-300 cm^{-1} region. These peaks match with a number of copper corrosion products (e.g. Cu_2O and CuO), so no specific products can be distinguished from them. The magnitude of the peaks in the region attributed to Cu_2O (100-200 cm^{-1}) is greater than that attributed to CuO (200-300 cm^{-1}), which may be indicative of the relative amounts of the two products. Peaks centred at 700 and 1000 cm^{-1} are also apparent in some spectra. These peaks do not appear to match the reference spectra for common copper corrosion products.
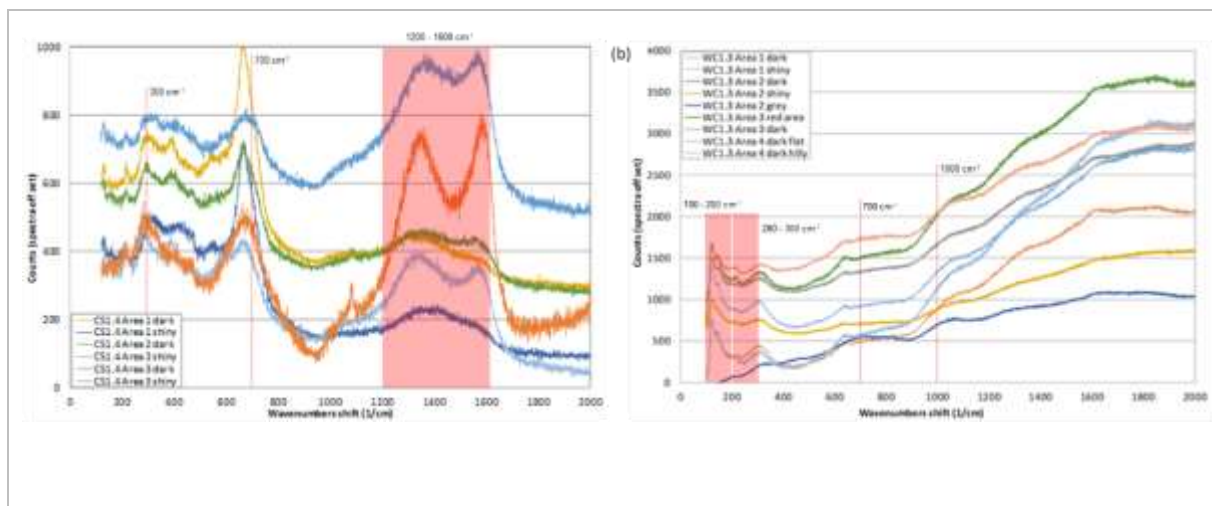
Figure 8. Raman spectra after in situ exposure for 394 days in bentonite with a density of 1250 kg m^{-3}, (left) carbon steel, (right) wrought copper.

The surface elemental concentrations obtained by XPS analysis from three points on a carbon steel and on a wrought copper coupon are shown in Table 1 and Table 2, respectively. On carbon steel, the main components of the surface were iron, oxygen and carbon. At least a component of the carbon signal was considered 'adventitious', as suggested by its rapid decrease during ion bombardment. The presence of Na, Ca, Mg, S and Al in modest concentrations in most measurements was attributed to dried groundwater (the lack of Si signal suggests that these areas may not contain bentonite solids). Silicon and aluminium were also detected in substantial quantities (7-8 at%) in one area, indicating adhering bentonite. The deconvolution of key peaks after ion bombardment and removal of adventitious carbon indicated that Fe was either in Fe(II) form (45 at.%) or Fe(III) form (50 at.%). The remaining 5 at.% was associated with FeS_2 as also indicated by the S spectrum. Oxygen was associated with oxides (iron corrosion products) and silicates (bentonite) (60 at.% and 40 at.% respectively). Carbon was associated with carbonate (100 at.%).

On the wrought copper, the most abundant elements were oxygen, silicon and carbon. As in the case of the carbon steel coupon, at least a component of the carbon signal was considered adventitious, as suggested by its rapid decrease after surface bombardment. The strength of the silicon signal (much stronger than in the case of carbon steel), however, suggests the presence of adhering bentonite solids on most of the surface. Other species found in lesser quantities (Na, Ca and Mg) could be also associated with such solids or with dried groundwater. More importantly, the copper signal was low (< 1 at.%), suggesting that XPS has been largely probing areas of adhering bentonite or altered phases not associated with corrosion products. Additionally, it is likely that the majority of the oxygen measured by XPS was associated with bentonite.

There was very little change in the copper peak position before and after ion beam bombardment, indicating a homogenous through-thickness composition. Within the tenuous copper signal measured, deconvolution of the XPS peaks showed a single oxidation state at ~933 eV, corresponding to Cu(0) or Cu(I). However, the lack of a significant satellite peak in the 943-947 eV region indicated that the species is predominantly metallic, suggesting that, if any corrosion product was present at all, such corrosion product would have been extremely thin (as the sampling depth for XPS is only a few nm). The entirety of the oxygen signal was attributed to silicates (rather than to oxides), consistent with observations on the copper signal (i.e. metallic copper). All the carbon signal, which was much smaller than in the case of carbon steel) was attributed to adventitious carbon, suggesting that no carbonate was present in this case.

Table 1. Surface elemental composition from XPS analysis of carbon steel (bentonite density 1250 kg m^{-3}) at three different points on the surface. In the case of Point 3, measurements were carried out before and after depth profiling (dp), expected to have removed a surface thickness of 3.3 nm.

	Element (normalized at %)								
Point	Fe 2p	O 1s	C 1s	Mg 1s	Na 1s	Ca 2p	S 2p	Al 2p	Si 2p
1	15.5	52.3	27.1	1.6	1.3	1.5	0.7	-	-
2	9.9	51.8	17.2	1.5	1.8	1.3	0.4	7.6	8.5
3 Before dp	13.6	54.0	26.6	1.0	0.8	1.8	2.3	-	-
3 After dp	24.0	60.3	8.6	2.0	0.4	3.2	1.6	-	-

Table 2. Surface elemental composition from XPS analysis of wrought copper (bentonite density 1250 kg m^{-3}) at three different points on the surface and after depth profiling (dp), expected to have removed a surface thickness of 3.3 nm.

Point	Element (normalized at %)						
	Cu 2p	O 1s	C 1s	Mg 1s	Si 2p	Na 1s	Ca 2p
1	0.7	62.6	10.5	1.6	22.3	1.5	0.9
2	1.0	65.5	5.7	2.1	23.2	1.6	0.8
3 Before dp	0.8	65.8	5.9	2.0	22.9	1.7	0.9
3 After dp	1.0	68.8	-	3.0	24.2	1.1	1.9

3.4 Characterisation of cross-sections of metal coupons

Representative optical and SEM-EDX analysis results of cross-sectioned carbon steel and wrought copper coupons are presented in Figure 9 and Figure 10, respectively. The main features of the analysis of carbon steel (bentonite density 1250 kg m^{-3}) were as follows:

- Sulphur, silicon and aluminium were present close to the metal surface. Given the presence of Fe, it is possible that these regions are the result of interactions between the bentonite and the corroding steel, rather than being fragments of bentonite that remained attached to the coupon.

- Iron was found in some areas associated with O only (e.g. right hand side of the alteration layer in Figure 9). This suggests that in some regions corrosion products exist without being intermixed with bentonite phases. Using the Fe signal as an indicator, the thickness of the corrosion product layer was estimated at approximately 5 µm.

- There appeared to be calcium-rich regions close to the steel surface, a phenomenon that has been reported before [4,14].

The main features of the analysis of copper (bentonite density 1250 kg m^{-3}) were as follows:

- It was not possible to discern evidence of a widespread surface alteration layer.

- In specific areas, a thin (<< 1 μm) layer enriched in O, C and Si was present at the metal/resin interface. It is likely that the C and O signals were the result of the use of the mounting resin. It is also possible that the Si and O signals were associated with a thin, adhering bentonite layer (consistent with XPS measurements). Al seems to be present in few isolated particles, where a strong presence of O signal indicating that it is the result of sample preparation (alumina grit blasting).

- S was found only in contact with the copper surface in isolated areas and associated with sub-micron surface features, indicating a corrosion process.
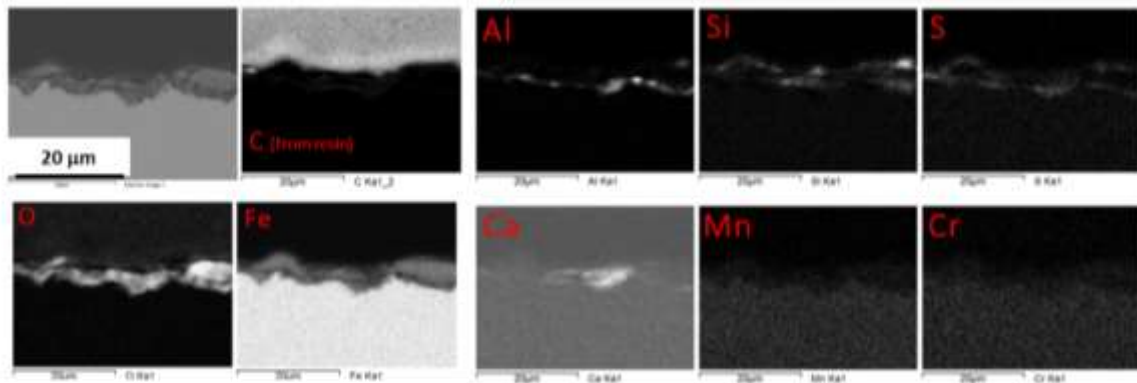
Figure 9. SEM image (top left) and EDX elemental maps of cross-section of carbon steel after in situ exposure for 394 days in bentonite with a density of 1250 kg m^{-3}.
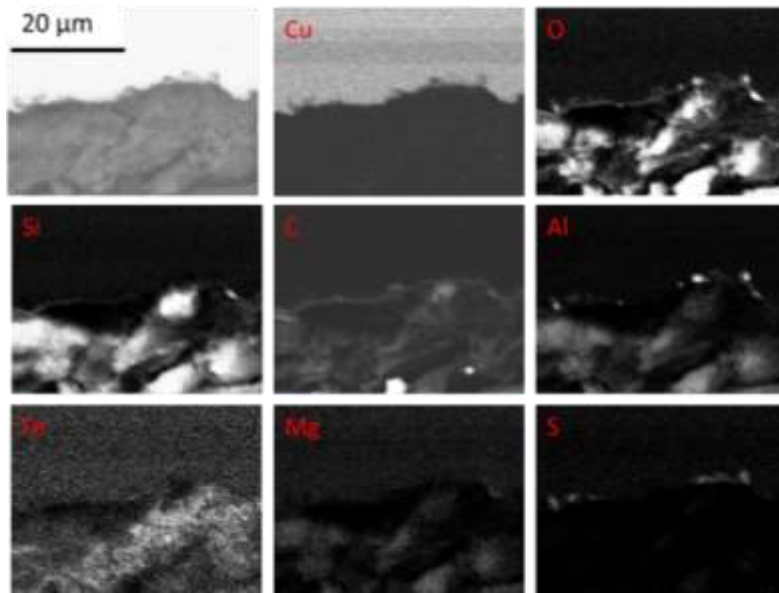
Figure 10. SEM image (top left) and EDX elemental maps of cross-section of wrought copper after in situ exposure for 394 days in bentonite with a density of 1250 kg m^{-3}.

3.5 Analysis of bentonite

Optical images of the bentonite surrounding carbon steel and wrought copper coupons after exposure are shown in Figure 11. The bentonite matrix immediately adjacent to the carbon steel coupon had a black colour, while it was stained with a reddish-brown colour over an area ~1 mm thick surrounding the coupon. For copper, the staining in the bentonite was much less, with some parts of the bentonite surface in direct contact with the copper appearing black but the staining did not penetrate into the bentonite matrix. No discoloration was found on the bentonite in contact with the stainless steel coupons.
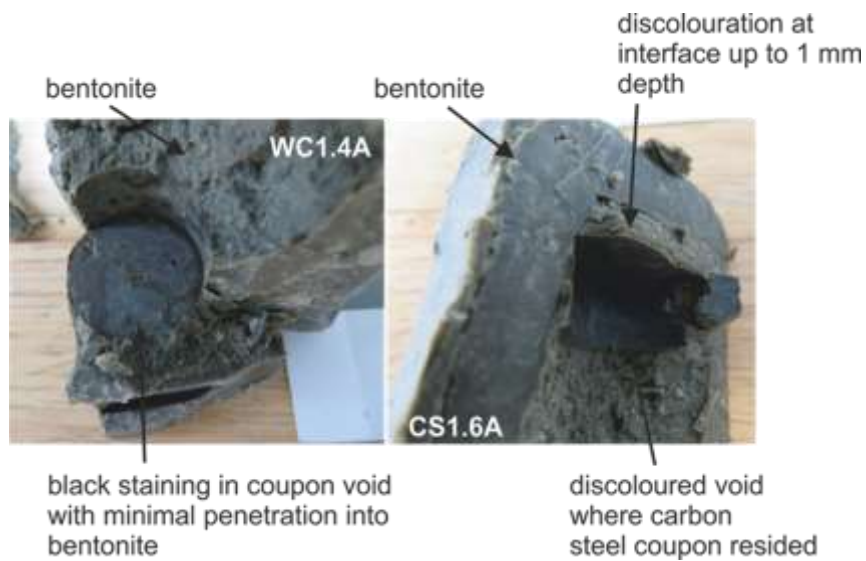
Figure 11. Visual appearance of bentonite with a density of 1500 kg m^{-3} surrounding wrought copper (left) and carbon steel (right).

SEM micrographs and EDX elemental maps of the bentonite-coupon interface for carbon steel are presented in Figure 12. A section of bentonite collected ~15 mm away from a carbon steel coupon is shown in Figure 13.
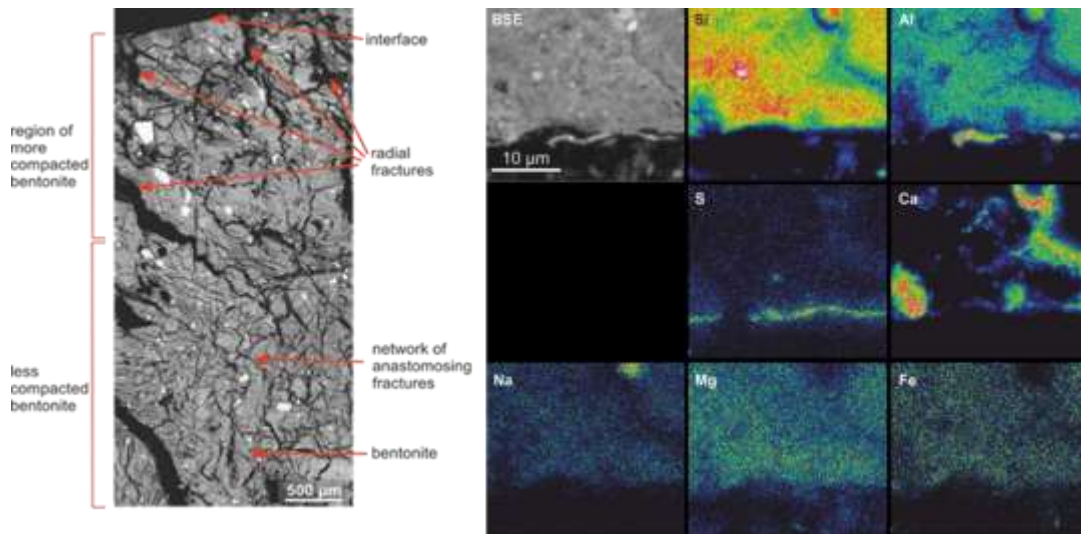
Figure 12. SEM image of bentonite next to the interface with a carbon steel coupon (left), and high magnification BSE image and corresponding EDX microchemical maps of the interface after in situ exposure of 394 (bentonite density 1500 kg m^{-3}) (right). Colour concentration scale: red > yellow > green > blue > black.
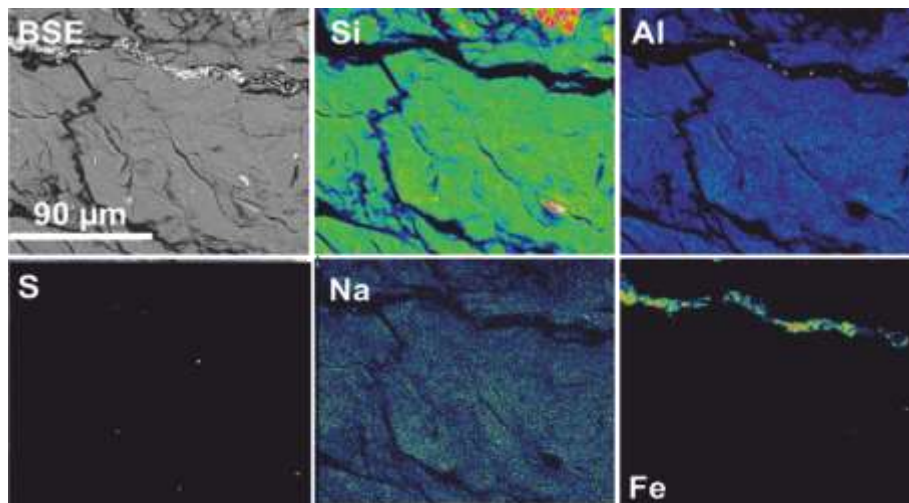
Figure 13. BSE high magnification image of a fracture within bentonite specimen collected ~15mmfrom steel interface (carbon steel, bentonite density 1500 kg m^{-3}) and corresponding EDX microchemical maps. Colour concentration scale: red > yellow > green > blue > black.

Bentonite had a difference in texture within ~2 mm of the steel surface (Figure 12, left). Adjacent to the interface, the bentonite appeared to be relatively densely-compacted, with radial shrinkage fractures. Most of these shrinkage fractures penetrated well beyond the visible brown stained halo (~1 mm from the interface). Some of this fracturing was probably created or enhanced by drying during sample preparation. Further into the bentonite matrix, the bentonite was noticeably less compact, and had a more open fabric containing an intense network of anastomosing microfractures formed sub-parallel to the interface surface. The bentonite also showed similar features and compaction within the first millimetre from the experimental cell (not shown), suggesting that such morphological changes are associated with mechanical effects and are not related with corrosion processes.

Along the interface of the bentonite with the carbon steel coupon, high-resolution mapping and BSE imaging revealed a thin layer lining the interface (Figure 12, right). EDX mapping showed that this was due to an enrichment in sulphur, with some corresponding, subordinate enrichment in aluminium and calcium. In other areas (not shown), regions rich in iron were found, which also contained sulphur, similar to what was observed for the distal section (see Figure 13). The geometry of these areas suggests that such regions may have been fractures filled with phases formed as a result of the evolution of the system, including iron released by corrosion processes.

Further away from the steel coupon (~15 mm, Figure 13), bright particles (<5 µm), identified by EDX as Fe-rich (probably Fe oxides), were lining fractures in the bentonite. These were concentrated on the distal side of the thin section and become less numerous towards the proximal side of the section. In some fractures, these particles were densely concentrated, completely infilling the pore space within the fractures. Interestingly, these particles contained no sulphur, which was only identified next to the metal-bentonite interface. The reason for this difference is currently unclear.

High magnification SEM cross sections EDX elemental maps of a cross section of the bentonite-copper interface are presented in Figure 14. The interface showed a 1-2 µm thick area characterised by a speckled, microgranular appearance, comprising the original smectitic clay (i.e. aluminium and silicon) but strongly enriched in copper and, to a lesser extent, sulphur. The oxygen signal overlapped with the Cu- and S-rich region, but it is not possible to assess if it originates in the bentonite or in the copper corrosion product. This layer was discontinuous along the full length of the interface. The bentonite texture close to the copper coupon was similar to the one close to the carbon steel coupon and the stainless steel filter (Figure 12, left), further confirming that this is primarily a mechanical effect, unrelated to corrosion.

Figure 15 shows SEM micrographs of the copper-bentonite interface, this time reproducing surface SEM images collected on an area of the bentonite previously in contact with a copper coupon. The images show that the alteration layer seen in Figure 14, consists of submicron particles rich in copper and sulphur interspersed in the bentonite. This finding is in agreement with the cross-section shown in Figure 10, where Cu-S-based particles were found adherent on the metallic surface.
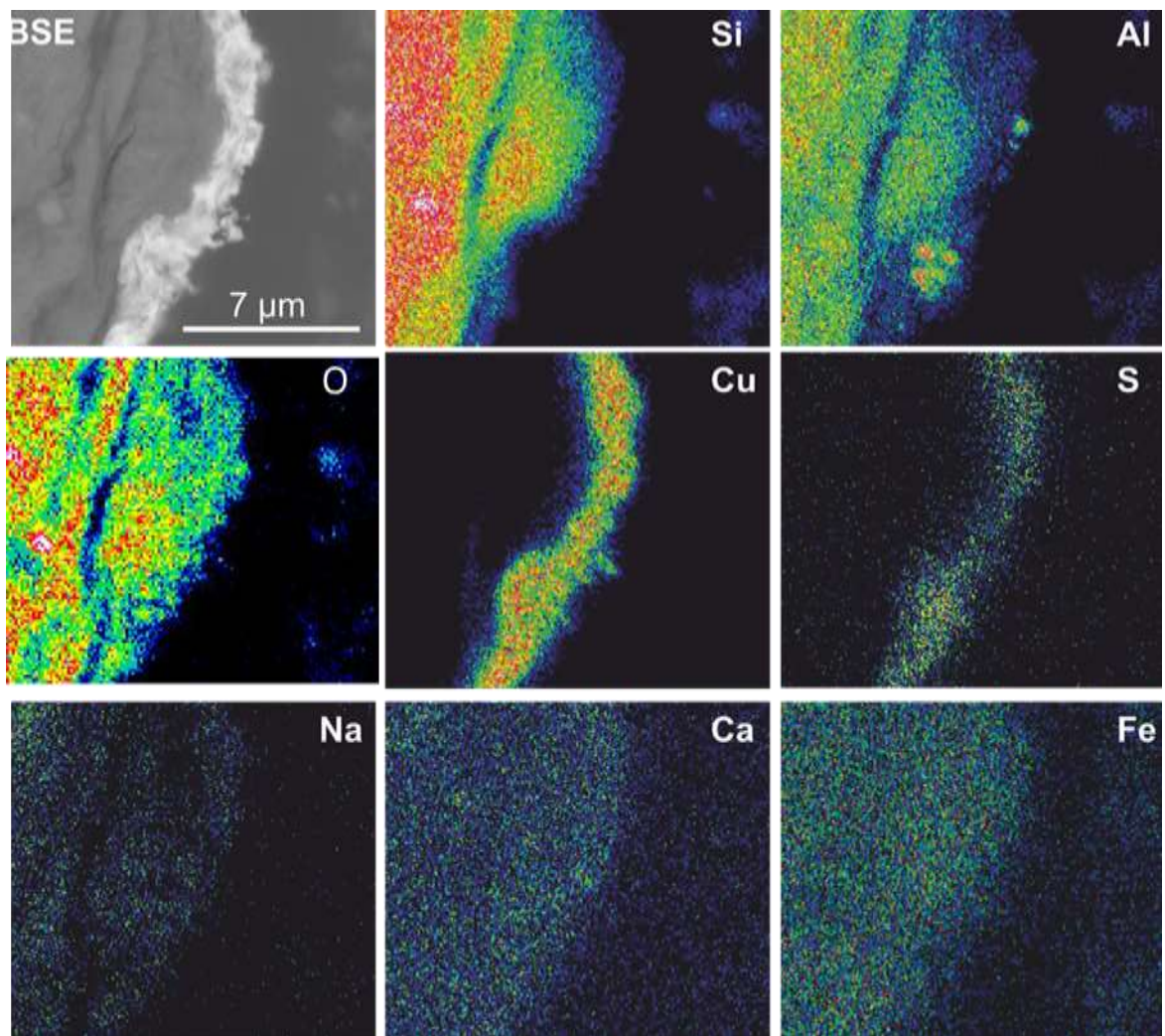
Figure 14. BSE image and corresponding EDX microchemical maps of bentonite specimen in contact with copper coupon (wrought copper, bentonite density 1500 kg m^{-3}). The mapped area is of the bentonite- copper interface. Colour concentration scale: red > yellow > green > blue > black.
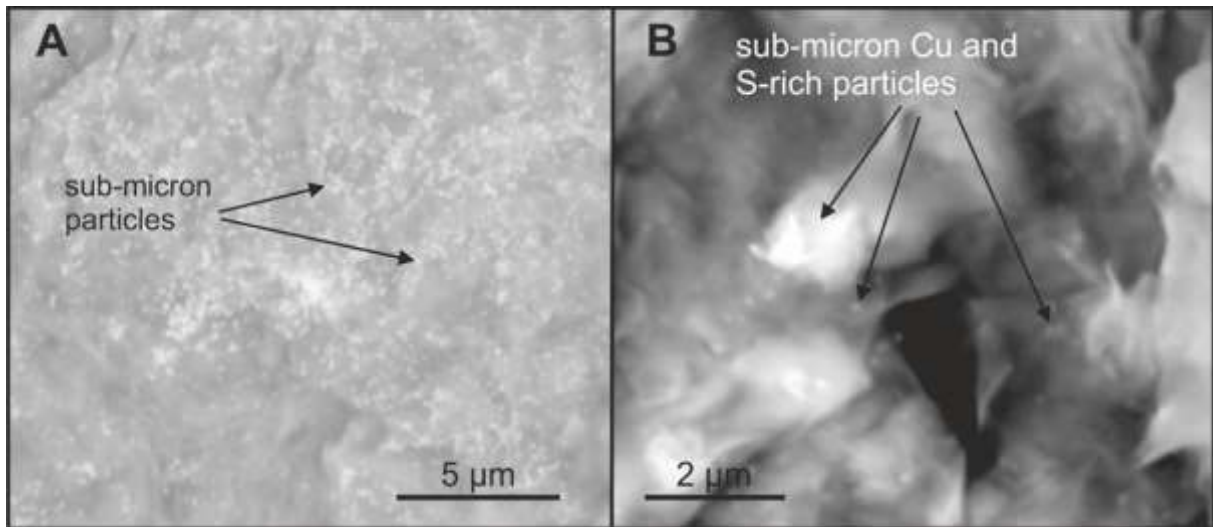
Figure 15. Surface BSE image of bentonite previously in contact with a copper coupon (wrought copper, bentonite density 1500 kg m^{-3}).

The XRD analysis on powdered bentonite in contact with both carbon steel and copper coupons (not shown) illustrated that the d_{060} plane was the same to that measured in bentonite in bulk bentonite, and in all cases produced values between 1.496 and 1.497 Å. This shows that no alteration of the dioctahedral structure of the montmorillonite occurred. However, XRD identified alunite ($KAl_3(SO_4)_2(OH)_6$) in the bentonite in contact with corroding wrought copper coupon. The primary reason for the formation of alunite could be an alteration of adherent alumina particles used for surface preparation due to reaction with the porewater.

4 Discussion

4.1 Corrosion rates

The average corrosion rate of carbon steel was approximately 1.96 µm yr^{-1}, with the corrosion rate being about 5% higher in bentonite with a density of 1500 kg m^{-3} compared to 1250 kg m^{-3}. These corrosion rates are comparable to those measured over similar durations in Opalinus Clay (1.2-2.1 µm yr^{-1} after 694 days) [12].

The average corrosion rate of the copper coupons, irrespective of bentonite density, was between 0.09 and 0.25 µm yr^{-1}, an order of magnitude lower than the carbon steel samples. Corrosion rates of copper were also similar to those found in the above mentioned experiment at Mont-Terri [14] (0.02-0.2 µm yr^{-1} after 1024 days). However, the measured rate was higher than those found, after longer emplacement periods, in Module 4 of the MiniCan experiment [31] conducted in the Aspö rock laboratory (0.02 µm year^{-1} after 9 years). Due to the possible ingress of oxygen during transport due to the damaged packaging, the reported corrosion rates may not be representative of totally anoxic conditions, even though they seem to agree with values from literature where oxygen was not a concern. Similarly, the surface roughness, R_a, for carbon steel and copper coupons after exposure is comparable to the values from the Mont Terri in situ experiment (1.0-1.4 µm for carbon steel after a period of 694 days, ~1 µm for copper after 1024 days [12]). The similarities between the corrosion rates in clay and granitic environments are probably due to the fact that the chemical environment at the coupon surface is primarily dictated by the bentonite, supported by the fact that the composition of the rock porewaters in Mont Terri and Grimsel are not significantly different [24,30]

Microbial analyses were conducted on the borehole water, the module canisters, the module filters, and the bentonite and reported elsewhere [11]. Enrichment of Pseudomonas stutzeri (aerobic heterotrophs) was observed in the outer layer of bentonite. Sulphate-reducing bacteria (SRB) Desulfosporosinus and Desulfovibrio were identified in the borehole water, with minor enrichment in the outer bentonite, but their presence did not extend to the inner bentonite. These bacteria can produce sulphide ions, but there is no evidence to suggest they were active in the bentonite. Any sulphide produced by the SRB may also become precipitate as mackinawite in the bentonite before it reaches the metal coupons [7]. No correlation between the microbial activity and the corrosion rates of the metal coupons was observed, indicating that MIC is not a significant contribution to material loss. Similar observations were made in the experiment carried out in Opalinus Clay host rock environment [12].

4.2 Metal coupon alteration

4.2.1 Carbon steel

The carbon steel-bentonite interface was characterized by a mixture of iron corrosion products and bentonite, as indicated by the presence of Fe and O signals, together with signals of other species arising from the bentonite. The presence of Fe and O in regions without Si (i.e. adherent bentonite) and the deconvolution of Fe peaks suggest the presence of iron oxides containing a mixtures of Fe(II) and Fe(III), identified as magnetite, haematite and iron oxyhydroxide by Raman spectroscopy. Other species of interest included carbonates and sulphur compounds, both not detected in the case of copper coupons. Mackinawite could have been formed by the reaction of iron released in the porewater by corrosion processes with sulphide present in the porewater [7], while pyrite is also present in the bentonite. However, the presence of Fe- and S-rich regions in fractures in the bentonite (Figure 13), and the fact that it was not detected on copper samples, suggest that the Fe-S compound detected on the carbon steel samples is likely to have been formed by corrosion processes, rather than being associated with pristine bentonite. Carbonate, e.g. siderite $Fe(CO_3)$, also absent on the copper samples and not present in substantial quantities in MX-80 bentonite, could also have originated from corrosion processes [32]. The presence of iron enrichment in the bentonite suggests that corrosion and alteration processes at the interface include migration of iron through the bentonite, as well as through microfractures.

4.2.2 Copper

A residual layer of bentonite was present on the copper surface after exposure, as evidenced by the presence of silicates. However, a faint copper signal (about 1 at.%) was detectable using XPS. Deconvolution of the peak associated with this signal indicated the presence of Cu(0) and potentially Cu(I). SEM/EDX cross section did not identify any clear evidence of a surface alteration layer on copper. However, weight loss measurements confirmed that a small amount of corrosion (10 – 250 nm) had occurred during exposure and Raman spectroscopy picked up signals associated with Cu_2O and/or CuO. It is possible that the absence of clear signs of copper oxides in XPS measurements and SEM/EDX cross sections is the result of the heterogeneity of the copper surfaces as well as of the limited de facto resolution of these techniques for the problem in question (in the case of SEM/EDX inherently associated with the technique and in the case of XPS associated with the modest copper signal measured, 1 at.%, as a result of adhering bentonite). The presence of reddish patches observed under visual examination would suggest that small amounts of copper oxides could have formed during the experiment.

Differently than in the case of carbon steel, no sulphur or carbonate were detected on the surface of copper using XPS. However, the SEM/EDX of cross sections indicated that a copper-containing bentonite phase and sparse submicron Cu-S-rich particles were present at the copper-bentonite interface. It seems likely that such phase and particles are a result of corrosion and remained adherent on the bentonite.

4.3 Bentonite alteration

The alteration induced by the bentonite-metal interactions did not alter the dioctahedral structure of the montmorillonite nor introduced any other mineralogical change. This observation is consistent with similar experiments reported elsewhere [33, 34]. The most obvious visual alteration feature in the bentonite is the red-brown discolouration of the bentonite matrix around the carbon steel coupon where the discolouration extends up to ~1 mm into the bentonite, which corresponds closely to the iron-enriched area seen in EDX analyses. Numerous Fe-rich particles were visibly lining microfractures within the bentonite matrix, indicating the presence of a well-connected fracture network throughout the bentonite matrix providing pathways along which the iron migrated away from the corroding metal coupon. The lining of some fractures by secondary precipitates suggests that at least these microfractures formed during the experiment (rather than as an artefact of sample drying). The corrosion of metals in anoxic conditions consumes water, which could have caused partial dehydration, shrinkage and the development of micro fracturing around the metal coupons.

In the case of copper, the formation of phases rich in Cu, S, and partly O, would appear to be responsible for the black staining on the bentonite contact surface, with the colour being consistent with a copper sulphide such as chalcocite (Cu_2S) or with a black copper oxide such as tenorite (CuO). The depth of this fringe was very limited and did not penetrate into the adjacent bentonite. The close correspondence of copper and sulphur would be consistent with the formation of a secondary copper sulphide phase. However, semi-quantitative EDX indicates Cu : S ratios that are considerably greater than the ratio of 2:1 expected for the simple cuprous sulphide, chalcocite (Cu_2S). Therefore, this secondary copper-sulphur-rich alteration product may be dominated by copper oxide with only a minor component of copper sulphide rather than a stoichiometrically simple single phase. Apart from enrichment in copper, the bentonite next to the coupons exhibited no other mineralogical or structural alteration.

5 Conclusions

Two modules containing carbon steel, copper and stainless steel corrosion coupons in contact with pre-saturated bentonite of two different dry densities, 1250 and 1500 kg m^{-3}, were exposed for 394 days to groundwater in an anoxic borehole drilled in granite. After retrieval, the surface of all metals was covered with adherent bentonite. The corrosion rate of carbon steel was ~2 μm year^{-1}, of copper 0.1-0.2 μm year^{-1}, and of stainless steel was below detection. The corrosion rates did not significantly vary with bentonite density or with the type of copper, and none of the metals exhibited any change in surface roughness after exposure. Furthermore, microbially induced corrosion did not appear to contribute measurably to the overall material loss. The carbon steel-bentonite interface was a mixture of corrosion products (magnetite, haematite, traces of Fe-S compounds, carbonate) and a Fe-enriched alteration layer extending approximately 5 µm into the bentonite. Visually, the bentonite was stained a red-brown colour

extending ~1 mm from the carbon steel surface, which coincided to an increased iron concentration. Fractures lined by iron-rich particles were found up to ~15 mm from the coupon, probably resulting from Fe-bearing fluid produced by corrosion passing along an interconnected microfracture network. No corrosion product layer could be identified on copper. However, some Cu_2O may have been detected on the surface, and fine submicron Cu-S particles were found in the bentonite up to 1-2 µm from the metal surface. The bentonite adjacent to the copper coupon exhibited only very superficial discoloration at the interface, probably linked to the presence of the Cu-S particles. Apart from enrichment with corrosion products, no other mineralogical or structural alteration of bentonite could be identified in the vicinity of carbon steel or copper coupons. No corrosion, alteration or bentonite discoloration was found for stainless steel.

6 References

1. Nagra, *The Nagra Research, Development and Demonstration (RD&D) Plan for the Disposal of Radioactive Waste in Switzerland, Nagra Technical Report NTB 16-02,* **2016**.

2. Radioactive Waste Management (RWM), *Geological disposal: Engineered barrier system status report,* DSSC/452/01, RWM, **2016**.

3. R. Patel, C. Punshon, J. Nicholas, P. Bastid, R. Zhou, C. Schneider, N. Bagshaw, D. Howse, E. Hutchinson, R. Asano, F. King, *Nagra Technical Report TR-12-06*, **2012**.

4. A. Jenni, P. Wersin, T. Thoenen, B. Baeyens, A. Ferrari, T. Gimmi, U. Mäder, P. Marschall, W. Hummel & O. Leupin. Bentonite backfill performance in a high-level waste repository: a geochemical perspective, *Nagra Technical Report NTB 19-03*, **2019**.

5. C. Padovani, F. King, C. Lilja, D. Féron, S. Necib, D. Crusset, V. Deydier, N. Diomidis, R. Gaggiano, T. Ahn, P. G. Keech, D. D. Macdonald, H. Asano, N. Smart, D. S. Hall, H. Hänninen, D. Engelberg, J. J. Noël & D. W. Shoesmith *Corrosion Engineering, Science and Technology, 52,***2017.**.

6. C. Padovani, B. Reddy, A. Rance, N. Smart, S. Swanton, J. Schofield, A. Milodowski, L. Field, S. J. Kemp, N. Diomidis, A. Martin, A. J. Johansson, R. J. Winsley, M. Cowley, presented at WM2020 Phoenix, AZ, USA, 8 March – 12 March, **2020**.

7. V. Cloet, M. Pekala, P. Smith,P. Wersin, N. Diomidis, An evaluation of sulphide fluxes in the near field of a HLW repository. *Nagra Technical Report NTB 17-04*, **2017.**

8. M. Birgersson, L. Börgesson, M. Hedström, O. Karnland, U. Nilsson, *SKB Report TR-09-34*, **2009**.

9. Y. El Mendili, A. Abdelouas, J.F. Bardeau, *Phys. Chem. Chem. Phys.* **2013** *15(23)*, 91.

10. A. Bengtsson, K. Pedersen., *Applied Clay Science*, **2017**, *137*, 203.

11. K. Engel, S.E. Ford, S. Coyotzi, J. McKelvie, N. Diomidis, G. Slater, and J. D. Neufeld, *American Society for Microbiology (M sphere)*, **2019** *4*, 6.

12. N. R. Smart, B. Reddy, A. P. Rance, D. J. Nixon, M. Frutschi, R. Bernier-Latmani. N. Diomidis, *Corrosion Engineering, Science and Technology* **2017**, *52:sup1*, 101-112.

13. N. Diomidis, B. Reddy, R. Bernier-Latmani. Corrosion of carbon steel in anaerobic saturated bentonite: in situ and ex situ experiments. Part 1. *Nagra Technical Report NAB 20-10*. **2020**.

14. B. Reddy, C. Padovani, A. Cook, N.R. Smart1, A.P Rance, A. Milodowski, L. Field, S. Kemp, A. Martin, N. Diomidis, Further results on the in situ anaerobic corrosion of carbon steel and copper in compacted bentonite exposed to natural Opalinus Clay porewater containing native microbial populations, *Materials and Corrosion*, In press.

15. S. Necib, N. Diomidis, P. Keech, M. Nakayama, *Swiss J. Geosci.,* **2017** *110*, 329-342.

16. N. Burzan, R. Bernier-Latmani, N. Diomidis. 2020. *Temporal evolution of the microbial community associated with Wyoming bentonite MX-80 saturated with Opalinus Clay rock porewater in situ*. In preparation.

17. S. Aggarwal, V. Addepalli, and N. Smart, *Swedish Nuclear Fuel and Waste Management Company Report, SKB R-15-11*, **2015**.

18. L. Hallbeck, L. Johansson, J. Edlund, and K. Pedersen, *Swedish Nuclear Fuel and Waste Management Company Report, SKB TR-16-13* **2017**.

19. Smart, N.R. and A.P. Rance. *Swedish Nuclear Fuel and Waste Management Company Report, SKB TR-09-20*, 2009.

20. N.R. Smart, A.P. Rance, B. Reddy, L. Hallbeck, K. Pedersen, and A.J. Johansson. *Corros. Eng. Sci. Tech.*, **2014**, *49,* 548-553.

21. P. Keech, P. Lin, N. Mahalanobis, presented at *CNS 2015*, New Brunswick, Canada 31 May – 3 June, **2015**.

22. P. Keech, P. Vo, D. Poirier J. G. Legoux, presented at *CNS 2015*, New Brunswick, Canada 31 May – 3 June, **2015**.

23. SKB, *Design, production and initial state of the canister*, *SKB TR-10-14*, **2010.**

24. R. Schneeberger, F. Kober, G. W. Lanyon, U. K. Mäder, T. Spillmann, I. Blechschmidt, *Nagra Technical Report TR-19-01*, **2019**.

25. ASTM-G1, S*tandard Practice for Preparing, Cleaning, and Evaluating Corrosion Test Specimens*, ASTM International, West Conshohocken, PA, US, **2011.**

26. E. Park, J. Zhang, S. Thompson, O. Ostrovski, R. Howe, *Metall. Mater. Trans. B.* **2001**, *32*, 839.

27. J. E. Castle, Practical Surface Analysis by Auger and X-Ray Photoelectron Spectroscopy, *John Wiley and Sons Inc,* Chichester, UK **1983**.

28. R. O. Ansell, T. Dickinson, A. F. Povey, P. M. A. Sherwood, *J. Electroanalytical . Chemistry* **1979**, *98(1)*, 79.

29. F. T. Madsen, *Clay Minerals*. **1998**, *33*, 109.

30. N. Diomidis, Scientific basis for the production of gas due to corrosion in a deep geological repository, *Nagra Technical Report* NAB 14-21, **2014.**

31. A. Gordon, L. Sjogren, C. Taxen, A.J. Johansson, *SKB report TR-16-12* **2017**.

32. N. R. Smart, B. Reddy, A. P. Rance, D. J. Nixon and N. Diomidis, *Corrosion Engineering, Science and Technology*, **2017**.*52:sup1*, 113-126

33. A. E. Milodowski, M. R. Cave, S. J. Kemp, H. Taylor, B. Vickers, K. A. Green, C. L. Williams, R. A. Shaw, *SKB Technical Report TR-09-02*, **2009**.

34. A. E. Milodowski, M. R. Cave, S. J. Kemp, H. Taylor, K. A. Green, C. L. Williams, R. A. Shaw, *SKB Technical Report TR-09-03*, **2009**.